Magnetostratigraphy of the late Cenozoic Laojunmiao anticline in the northern Qilian Mountains and its implications for the northern Tibetan Plateau uplift

FANG Xiaomin[1,2], ZHAO Zhijun[3,2], LI Jijun[2], YAN Maodu[2], PAN Baotian[2], SONG Chunhui[2] & DAI Shuang[2]

1. Institute of Tibetan Plateau Research, Chinese Academy of Sciences, Beijing 100085, China;
2. Key Laboratory of Western China's Environmental Systems, Ministry of Education & College of Resources and Environment, Lanzhou University, Lanzhou 730000, China;
3. College of Geography, Nanjing Normal University, Nanjing 210097, China

Correspondence should be addressed to Fang Xiaomin (email: fangxm@lzu.edu.cn)

Received May 22, 2003

Abstract Cenozoic sediments in the foreland basin——Jiuquan Basin in west Hexi Corridor recorded tectonic uplift information of the Qilian Mountains. High resolution paleomagnetic dating of the Laojunmiao (LJM) section across the central LJM anticline in the southern Jiuquan Basin reveals ages of the Getanggou Member, Niugetao Member in the Shulehe Formation, the Yumen Conglomerate, Jiuquan Conglomerate and Gobi Formation at >13—8.3 Ma, 8.3—4.9 Ma, 3.66—0.93 Ma, 0.84—0.14 Ma and 0.14—0 Ma, respectively. Sedimentary evolution study suggests that the Qilian Mountains should begin to rise gradually since ~8—6.6 Ma, accompanied by sedimentary environments changing from lacustrine mudstones-sandstones to alluvial conglomerates. Rapid uplift of the Qilian Mountains began at ~3.66 Ma, followed by a series of stepwise or intermittent intensive uplifts at about <1.8—1.23 Ma, 0.93—0.84 Ma and 0.14 Ma, which finally resulted in the present high Qilian Mountains.

Keywords: Qilian Mountains, Qinghai-Tibetan Plateau, Jiuquan Basin, magnetostratigraphy.

DOI: 10.1360/03yd0188

The uplift process of the Qinghai-Tibetan Plateau holds the key to understand the dynamic mechanisms of continental crust shortening and mountain-building and to test the relationship between the Tibetan uplift and tectonic-climatic coupling and environmental impacts[1—4]. However, there are still many debates in the process and mechanism of how the Tibetan Plateau uplifted to the present configuration. Among various approaches to solve these key questions, dating of the Cenozoic stratigraphy in foreland basins around the margin of the Tibetan Plateau is of great significance. Any surface uplift of the Plateau will enlarge relief, which should be recorded directly by sediments in related basins. Only tectonic-caused surface uplift is of our interest here. By dating the absolute ages of the Cenozoic foreland stratigraphy of the Siwalik Group, and deciphering signals of tectono-sedimentary environmental changes, the uplift history of the Himalayas has been reconstructed[1,2]. However, less work has been done in the northern Tibetan Plateau. Two exceptional cases come from the works in the northeastern and northwestern Tibetan Plateau[5—8]. The former has

reconstructed the evolution of the northeastern Tibetan Plateau since 29 Ma, based on detailed chronology and environmental studies supported by the National Tibetan Project in the Chinese 8th Five-Year Plan in Science, which demonstrates that the northeastern Plateau began to uplift rapidly at ~3.6 Ma[6,7]. The latter measured a long section at Yecheng in the southern Tarim Basin and showed that the West Kunlun Mountains underwent a rapid uplift also at ~3.6 Ma[8]. However, evidence only from the two localities are too few to allow the reconstruction of process of uplift of the entire Tibetan Plateau, more locations are needed. The Cenozoic stratigraphy in the foreland Hexi Corridor is a key locality, where it is right situated at the central part of the principal stress of the N-S compression——a place still tectonic active in present day[9−11]. Nevertheless, one of popular models believes that the uplift process of the NE Tibetan Plateau might differ from that of the main Plateau south of the Kunlun Mountains. The NE Tibetan Plateau may be formed from a northeastern accretion of a large scale upper crust decollement decoupled from the lower crust and mantle, which is controlled by a co-action of the Kunlun strike slip and the Altyn Tagh strike slip faults[11,12]. Here we make very detailed magnetostratigraphic study in the most representative basin — the Jiuquan Basin in the northern Tibetan Plateau (Fig. 1), with an attempt to focus on the well-known Yumen conglomerates and other related tectonic events.

1 Geological setting

The Hexi Corridor is a foreland basin, defined by the NWW northern Qilian Mountains fault to the south and the Longshou Shan fault to the north (Fig. 1). It is further dismembered into several sub-basins by a group of active NNW-NW dextral transpressional sub-faults and their controlled upheavals. For example, the Wenshu Shan upheaval and the Jiayuguan fault divide the Jiuquan Basin into the Jiuxi Basin and Jiudong Basin, the Yumu Shan upheaval and the Yumu

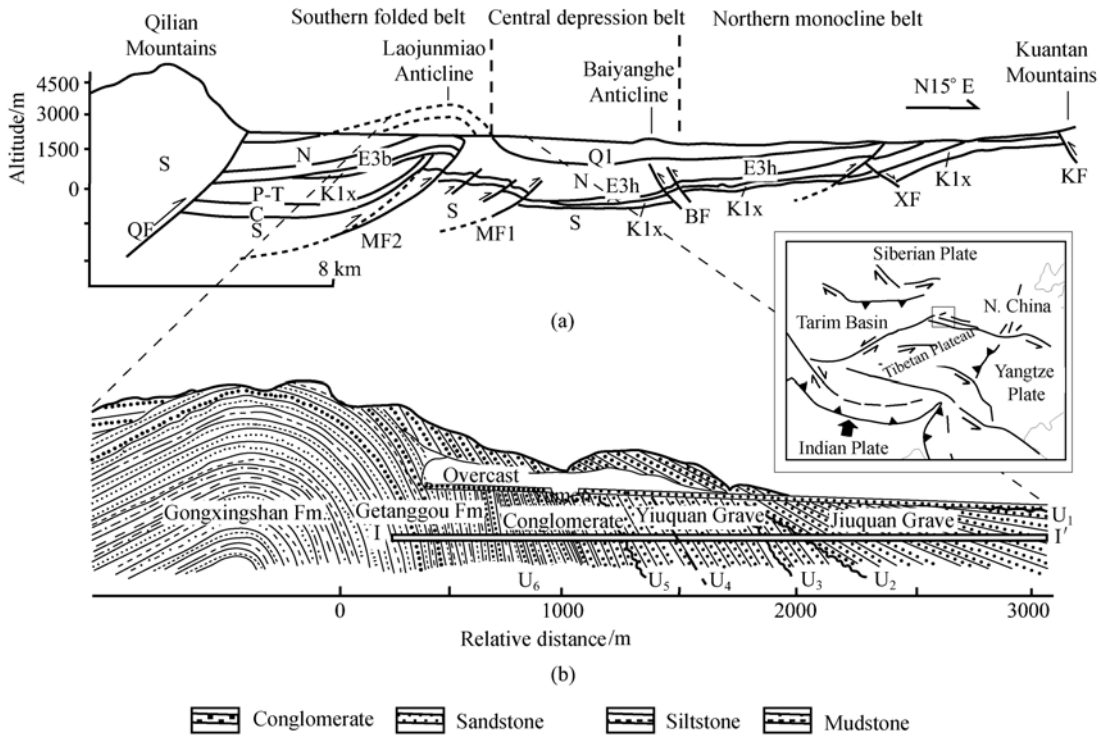

Fig. 1. Tectonic location and N-S cross section of the Jiuxi Basin (a) and the Laojunmiao anticline (b). MF1 and MF2, Miaobei No.1 and No. 2 faults; BF, Bainan fault; XF, Xinminbao fault; QF, Northern Qilian Mountains fault; KF, Kuantan Shan fault; S, Silurian; C, Carboniferous; P-T, Permian to Triassic; K1x, Lower Cretaceous; E3h, Huoshaogou Fm; E3b, Baiyanghe Fm.; N, Shulehe Fm; Q1, Yumen Conglomerate; I-I′, the sampling profile.

Shan fault separates the Jiudong Basin and the Mingle Basin, and the Dahuang Shan borders the Mingle Basin and the Wuwei Basin.

The Jiuxi Basin is a sedimentary basin located at the westest Hexi Corridor. It is delineated by the Qilian Mountains to the south, the Chijin Gorge—Kuantan Shan—Hei Shan to the north, the Xiaohongliu Gorge to the west, and the Jiayuguan—Wenshu Shan to the east. Tectonically it is directly controlled by the northern Qilian Mountains thrust fault and Altyn Tagh strike slip fault (Fig. 1). The sedimentary sequences completely recorded the tectonic uplift process of the northern Qilian Mountains. The basin can be tectonically divided in three zones: the southern upheaval, the central syncline depression consisting of Cenozoic stratigraphy, and the northern monoclinal slope of Eogene base rocks (Fig. 1). The southern upheaval zone is of great interest. It consists of a series of NW anticlines involving mostly the late Cenozoic stratigraphy and the Yumen conglomerates (Fig. 1). In geomor--phology, the Jiuxi Basin is contrast to the Qilian Mountains by large different elevations. The basin-surface is at altitudes of 2000－2300 m, while the Qilian Mountains stands up to over 4500 m a.s.l. (Fig. 1).

2 Section and stratigraphy

Although stratigraphy of the Hexi Corridor has been long studied, it is still poorly understood because of lacking accurate age constraints. In 1893, Russian geologist Obuluchev investigated Gansu and named the Tertiary stratigraphy “Hanhai System”[13]. In 1942, Sun Jianchu divided the Tertiary Gansu System into the Miocene Baiyanghe System and the Pliocene Shulehe System and thought that the huge thick gravels are Quaternary in age. He named the lower and upper gravels the Early Pleistocene Yumen Gravel Bed and the middle Pleistocene Jiuquan Gravel Bed. The Baiyanghe System was further subdivided upperwards into the Jianquanzi Member, Ganyouquan Member and Shiyougou Member, and the Shulehe System upperwards into the Gongxingshan Member, Getanggou Member and Niugetao Member[14]. In 1957, Yu Boliang renamed the Yumen Gravel Bed the Yumen Conglomerate according to its cementation and thought that its age should be Neogene and the age of the Jiuquan Gravel Bed should be also older[15]. In 1958, Song Zhichen pointed out that the Shulehe Formation should be the Pliocene in age and the Baiyanghe Formation may be the Miocene or Pliocene in age according to fossil pollen spores in the Jiuquan Basin[16]. Since 1993, preliminary paleomagnetic works were made for the Cenozoic stratigraphy in the basin[17—19], yielding rough ages generally agreeing with those suggested by fossil mammals. Because all these are largely based on estimations from stratigraphic relationship and also the obtained paleomagnetic ages have very big uncertainties due to very large sampling intervals and incomplete observed magnetic chrons, it is necessary to make a detailed systematic chronological study of the Cenozoic stratigraphy in the Hexi Corridor. Therefore, we chose the most representative late Cenozoic stratigraphic LJM anticline section in the Jiuquan Basin as our study area.

The LJM anticline, where the Chinese first petroleum borehole was drilled, is located at Yumen City (97°32′E, 39°47′N), belongs to one of the series of anticlines in the southern upheaval of the Jiuquan Basin (Fig. 1). It has a gentle southern side, but a very steep or even reversed northern one. The Shiyou River cuts northwards across the central anticline. From the core of the anticline to northward, there were exposed sequences of the Gongxingshan, Getanggou and Niugetao Members of the Shulehe Fm, the Yumen Conglomerate, the Jiuquan Gravel Bed and the Gobi Gravel Bed. The thickness of the section is 1960 m after tilt-calibrated. Six unconformities were observed in the section, numbered downwards as U_1 to U_6 located at depths of 20, 247, 310, 552, 754 and 1160 m, respectively. U_1 separates the Gobi Gravel Bed with the Jiuquan Gravel Bed, U_2 the Jiuquan Gravel Bed with the Yumen Conglomerate, U_3 the upper with middle Yumen Conglomerate, U_4 the middle with lower Yumen Conglomerate, U_5 the Yumen Conglomerate with the Shulehe Fm, and U_6 the upper with middle Shulehe Fm (Fig. 1(b)). Unconformities U_2, U_3 and U_5 are the most developed ones. U_1 is a partially developed unconformity and occurs only in the prox-

imity of fold and disappears outwards (northwards), where stratigraphy is conformable. U_4 is a disconformity without clear identified erosive surface but only manifests as obvious changes in size and alignment of gravels around the disconformity, where average maximum diameter of gravels suddenly changes from cobbles of 17—24 cm below the disconformity to boulders of 28—55 cm above. Statistics of the gravel dips show that the paleoflow directions changed from previous northwesterly to later disperse (or some northeasterly)[20]. Paleomagnetic study indicates there is a clear hiatus at the disconformity (see below). U_6 is broom-like and has no clear erosive discontinuous surface. It mostly manifests as a gradual change of stratigraphic dips from 80° at the depth of 1180 m to 68° at the depth of 1113 m (Fig. 1). Thus, it is not a common unconformity we used to, but a progressive unconformity reflecting a syntectonic sedimentation due to anticlinic progradation[21].

The measured Getanggou Member is >608 m thick (depths 1352—1960 m, bottom unseen) and is characterized by alternation of sandy conglomerate-sandstone-siltstone-mudstone cycles (each 30—40 m thick). The cycles in the lower 112 m of the Member are smaller and the sandy conglomerate-sandstone beddings are very thin or even missing, and it is predominated by interbeddings of siltstones and brownish red mudstones with horizontal bedding, small sand ripple bedding and many vertical fossil animal tubules. The sandy conglomerate and sandstone are poorly sorted, supported by matrix, developed graded bedding, sand gravel rhythmic bedding or massive bedding (but lacking of cross-beddings), and have quick spatial changes, suggesting a fast deposition of subaqueous mass flows.

The Niugetao Member is 598 m thick (depths 754—1352 m). Its lower part (depths 1113—1352 m, 239 thick), consists mainly of sandy conglomerate-coarse sandstone-siltstone, occasional with thin mudstone, characterized by poor sorting, matrix-supporting, rough parallel bedding, graded bedding and sand-gravel rhythmic bedding, less vertical fossil tubules, and even reworked paleosols (only at depth 830 m). Its middle part (depths 940—1113 m, 173 m thick) is mainly of huge thick sandy conglomerate or gravelly sandstone, intercalated with thin muddy sandstone, has sedimentary features similar to that in the lower; Its upper part (depths 754—940 m, 186 m thick) is characterized by huge thick conglomerate with obvious matrix-supported, massive or roughly graded beddings, intercalated with poorly sorted sandstone belts.

The Yumen Conglomerate is 507 m thick (depths 247—754 m), with poorly sorted gravels, commonly 3—5 cm (maximum 40—50 cm) in diameter and generally subangular to subrounded. The gravels in the lower part have relatively unified size, but in the upper part are angular and have stone line structure and grouped (bag-like) structure interbedded with sand lens.

The Jiuquan Gravel Bed is 227 m thick (depths 20—247 m) and is divided into lower and upper parts. The lower part is 201 m thick and very poorly sorted and the enclosed gravels are generally 5—7 cm (maximum 40—50 cm) in diameter. The upper part is only 26 m thick. Compared with the Yumen Conglomerate, the dark gray color of the Jiuquan Gravel Bed is much darker.

The Gobi Gravel Bed consists of gravels of generally 7—10 cm (maximum 50—70 cm) in terraces 1 to 3 of the Shiyou He (River) and has a thickness of 20 m (depths 0—20 m).

Generally, from the bottom to the top of the section, the proportion of sandy conglomerate and conglomerate increases, and the maximum diameter of the enclosed gravels increases as well from about 6 cm to 50—70 cm.

3 Paleomagnetic sampling and measurement

Because the stratigraphy has developed unconformities and lacks other independent reliable absolute age constraints, to make high dense sampling sites becomes a key to protect the existing magnetic zones from absence. Experience from the Linxia Basin shows that 2 m equal intervals could guarantee an observation of most ten thousand year scale magnetic

chrons. Thus, 2 m sampling intervals (some at 2—5 m intervals in conglomerates in the upper section) were taken for this study and we believe this sampling interval would be dense enough to get most magnetic chrons since the sedimentation rate in the studied region is much higher than that in the Linxia Basin. In the lower section, samples were largely made on mudstones and siltstones, while in the upper section, only lenses of mudstones, siltstones and sandstones are chosen for sampling. Three cubic samples at 2.2 cm×2.2 cm×2.2 cm were taken at each site, forming three sets of samples (each for 522 ones). Total 1566 samples were collected.

Two sets of the samples were measured on the partially magnetically sheltered American 2G-755R cryogenic magnetometer in the Paleomagnetism Laboratory of the Institute of Geology and Geophysics of CAS, during which one set was AF-demagnetized and the other was thermal-demagnetized. Over 100 representative samples were chosen for systematic thermal demagnetization. Based on this, others were only partially (3—5 steps) demagnetized. The third set of the samples were measured also on 2G cryogenic magnetometer but equipped in a magnetically sheltered room in the Paleomagnetism Laboratory of the Department of Geological Sciences, the University of Michigan, U.S.A.. Thermal demagnetization was carried out in 18 steps between 25℃ and 685℃.

Figure 2 shows thermomagnetic behaviors of some representative samples. Most thermal-demagnetized samples show a quite similar thermomagnetic pattern, that is, the remnant intensity and direction have clear changes at about 200℃ with the removal of the secondary remanence. After 300—400℃, some even only after 500℃, remnant directions become stable toward the coordinate origin. The corresponding remnant

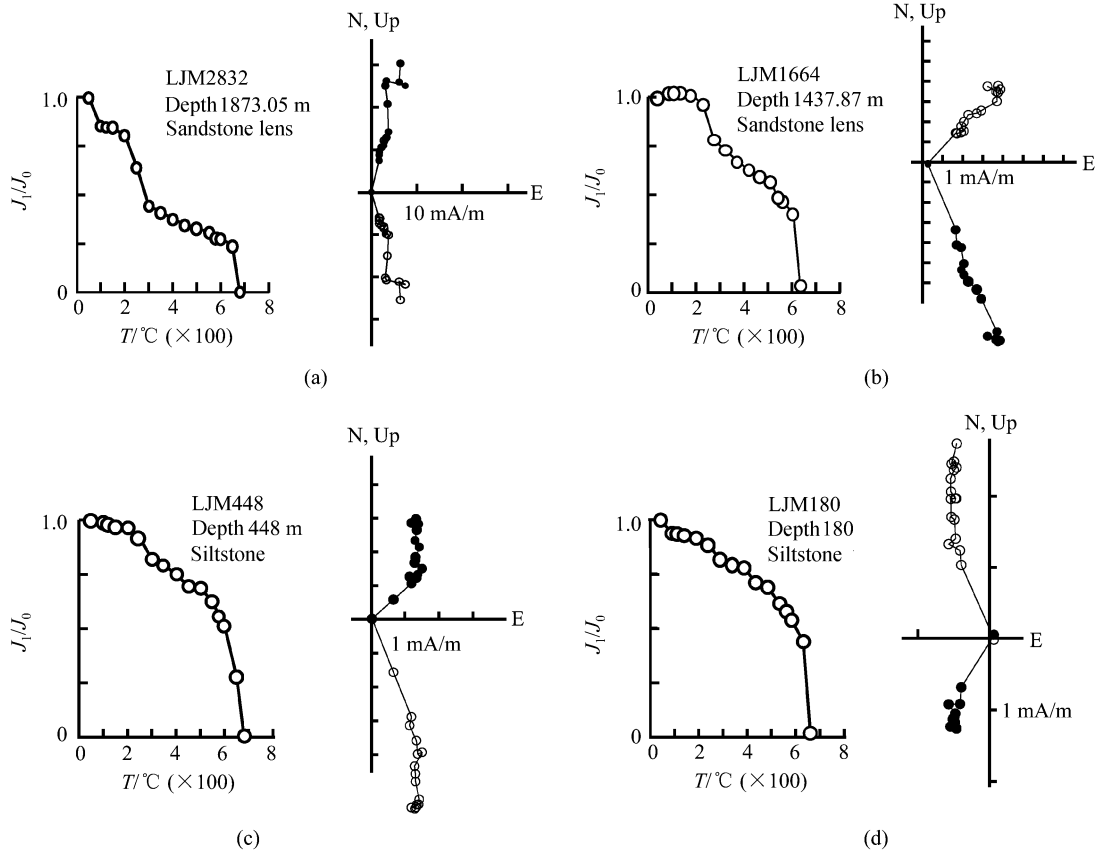

Fig. 2. Stepwise thermal demagnetization of some representative samples in the Laojunmiao section. Results are plotted in normalized NRM decay curves (left) and Zijderveld diagrams (right). Solid (open) circles in Zijderveld diagrams indicate declinations (inclinations).

intensity shows a gradual decay, then at about 580℃ a small but sudden fall, and finally decay to zero around 685℃ (Fig. 2). This indicates that the characteristic remanence (ChRM) is isolated after 300—400℃ for most samples. Many samples, especially those from silt and sand lens in conglomerate or gravel beds, the remanences have a clear decrease in intensity and a change in direction at about 250—400℃ after removal of the viscous remanence, then show a similar pattern like other samples described above (Fig. 2(a)—(c)). Therefore, it is estimated that the ChRM is most possibly carried chiefly by hematite and partially by magnetite and the secondary viscous remanence may be possessed by maghemite. As Hematite is the main remnant magnetization carrier, AF demagnetization results are not good, which is not shown here.

The IRM acquisition and back field measurements of some representative samples show that the IRM increases very fast below 0.2 T, and then very slow until 2.3 T, at which the IRM still has not reached its situation (Fig. 3(a), (b)). This pattern is most distinctive in mudstone and siltstone samples (Fig. 3(b)). Similar changes are observed in the coercivity curve in the back field measurement, but reversed (Fig. 3(a), (b)). Both changes determine the values of M_r and H_{cr} for sandstones at about 4—6 A/m and 50—70 mT, respectively, and for mudstones-siltstones at about 1—2 A/m and 90—120 mT, respectively. All these demonstrate that sandstones and siltstones-mudstones contain a small proportion of strong magnetic minerals and a large amount of weak magnetic minerals. Combined with their thermomagnetic behaviors above (Fig. 2(a), (d)), we estimate that the strong magnetic minerals are largely magnetite and maghemite, while the weak ones are hematite. Therefore, the main magnetic minerals carrying the remanences in sandstones are chiefly hematite and partially magnetite and maghemite, while in mudstones-siltstones is largely hematite. This is further confirmed by low and high temperature-dependent magnetic susceptibilities of the samples. The low temperature susceptibility of

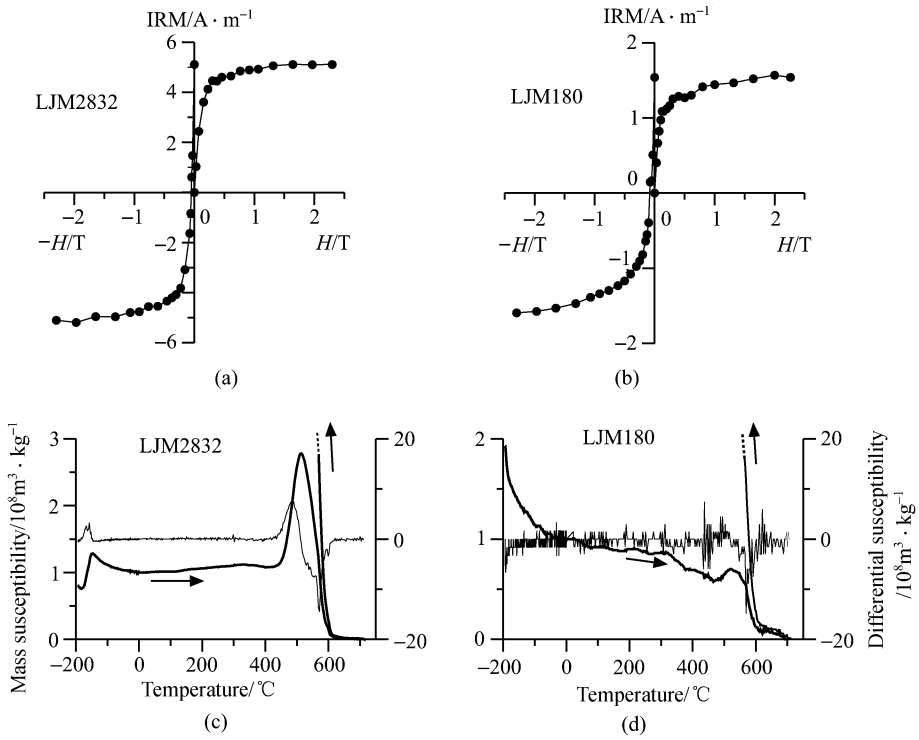

Fig. 3. IRM acquisition curves ((a), (b)) and temperature-dependent magnetic susceptibility measurements ((c), (d)) for some representative samples in the Laojunmiao section. Solid lines in c and d indicate magnetic susceptibility normalized by value at 0℃; while fine lines indicate differential magnetic susceptibility calculated from the differences between each two values of the susceptibility.

sandstone has a rapid increase at the Verwey transform point of magnetite at about −150℃, whereas at high temperature (300℃) the susceptibility decreases until near the Curie temperature of magnetite at 580℃, at which the susceptibility rapidly increases followed by a sudden drop to near zero, but decreases completely to zero only at the Curie temperature of hematite at 680℃ (Fig. 3(c)). This may indicate the existence of magnetite and hematite respectively in order. For siltstones-mudstones, no Verwey transform is observed, but rather an exponential decrease of the susceptibility with increase of temperature. Their high temperature susceptibilities are similar in behavior to those of sandstones above, but with weaker Hopkinson effect, subsequent smaller drop and steeper slope to zero at the hematite Curie temperature (Fig. 3(d)), suggesting a much higher presence of hematite than sandstones above.

About 25% of the total samples present unstable or no ChRM directions during thermal demagnetization. But supplemented by two times of re-sampling, only ~2% of the samples show such behavior, thus discarded. The ChRM directions of the remaining samples were obtained using principal component analysis. Mean direction for each site was obtained by Fisher-averaging and then virtual geomagnetic polarity (VGP) was calculated. For those with (1) ChRM directions revealed maximum angular deviation (MAD) angles greater than 15°; and (2) specimens revealed that magnetizations with virtual geomagnetic pole (VGP) latitude values less than 30° were rejected in the magnetostratigraphic column. A total of 80 sampling sites (15.3%) in the LJM section were excluded. All the paleomagnetic data passed the fold test[22] (set n=522, K1/K2=5, all the data passed F-test at 95% confidence), indicating that ChRM directions were acquired before folding. We used a statistical bootstrap technique[23] to examine possible non-Fisherian distributions of ChRM vectors, and to characterize the associated uncertainties for both normal and reversed ChRM directions, as illustrated in Fig. 4(b). The histograms of Cartesian coordinates of bootstrapped means[23] allow us to determine a 95% level of confidence (ovals around the means in Fig. 4(a)) and demonstrate that the bootstrap reversal test is positive (Fig. 4(b)). Finally, we used the jackknife technique[24] to quantify the reliability of the magnetostratigraphy (Fig. 4(c)). The obtained jackknife parameters (J) has a value of –0.2217 in the LJM section, which indicates that sampling of the section has recovered more than 95% (Fig. 4(c)).

4 Magnetic polarity stratigraphy

In total, 21 normal polarity zones (N1—N21) and 21 reversed polarity zones (R1—R21) were detected in the section. Most of these can be correlated with the geomagnetic polarity timescale (GPTS) of Cande and Kent[25] (Fig. 5).

The long-normal zone N1 and the short reversal period R1a can be correlated to the Brunhes and the uppermost Matuyama chrons, because the section above U2 is continuous to the present. This is confirmed by the ESR ages obtained at depths 116 m (0.19 Ma) and 164 m (0.61 Ma) from quartz sands extracted in sand-silt lenses in gravel beds[26] (Fig. 5), and also by detailed paleomagnetic dating of this part of the stratigraphy[27].

Because unconformities in the upper section create uncertainties in polarity correlation, firstly we make correlations for the middle and lower parts of the section below unconformity U_5, where the stratigraphy is continuous and long enough to enable correlation to the GPTS. We can then confine the age range of the unconformities, and make paleomagnetic correlations more reliable. Finally, independent ESR and fossil mammal-suggested ages are used for comparison and test.

Following this strategy, we can establish that the observed 14 normal magnetic polarity zones N8—N21 and 15 reversed ones R7b—R21 in the middle and lower parts of the section can be correlated to polarity chrons between 3n and 5Ar of the GPTS[25]. For example, the observed long normal zone N17 is correlated with the longest normal chron C5n of the GPTS since 15 Ma, the normal zones N9 and N10 can be corrected with the two sub-chrons C3An. 1n and

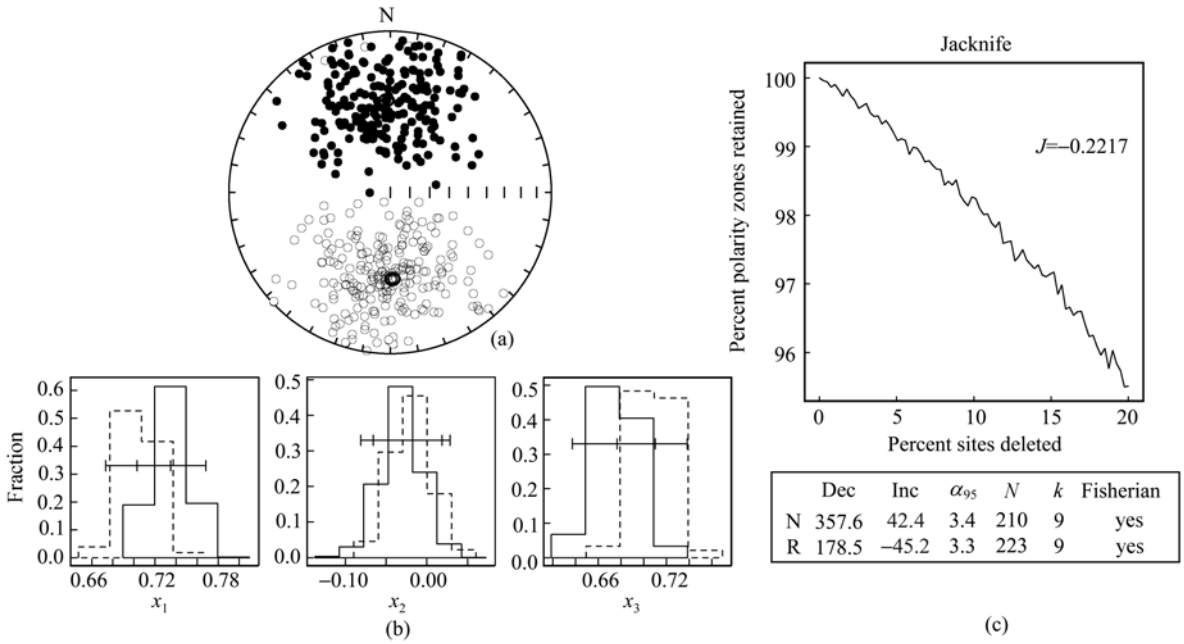

	Dec	Inc	α_{95}	N	k	Fisherian
N	357.6	42.4	3.4	210	9	yes
R	178.5	−45.2	3.3	223	9	yes

Fig. 4. (a) Equal-area projections of the characteristic remanent magnetization (ChRM) directions and mean directions (with oval of 95% confidence) determined with the bootstrap method[23]. Downward (upward) directions are shown as filled (open) circles. (b) Bootstrap reversal test diagram. Reversed polarity directions have been inverted to their antipodes to test for a common mean for the normal and reversed magnetization directions. The confidence intervals for all components overlap, indicating a positive reversal test. (c) Magnetostratigraphic Jacknife analysis[24] for the Laojunmiao section. The plot indicates the relationship between average percent of polarity zones retained and the percentage of sampling sites deleted, where the slope J is directly related to the robustness of the results[24]. The obtained slopes J have values of –0.2217 in the Laojunmiao section, which predicts that the section has recovered more than 95% of the true number of polarity intervals.

C3An.2n of chron 3An respectively; and the observed longest reversed zone R8 above N8 matches chron 3r of the GPTS (Fig. 5). Comparison of the observed zones in the middle and lower parts of the section with other time intervals of the GPTS would lead to poor correlations and unrealistic sedimentation rate changes. In contrast, our correlation determines a linear pattern of the sedimentation rates for these parts of the section (Fig. 6), which agree well with the stable environment suggested by the deposition of dominantly fine sediments during that time (Fig. 5). Thus the age of the corresponding stratigraphy is estimated between about 5 and 13 Ma (Fig. 5).

Accepting the interpretation above, the ages of the stratigraphy between the lowermost and uppermost unconformities are confined in about 5—0.8 Ma. Correspondingly, if it appears that the 5 normal zones N3-N7 and 6 reversed ones R2b—R7a can, by their structure, be correlated with chrons 1r —2Ar of the GPTS. Thus, the normal zone N2 and two reversed ones R1a—R2a are most possible analogs of the subchron 1r.1n (Jaramillo event) in the Matuyama reversed epoch (1r) and the partially remaining parts of 1r, respectively (Fig. 5). Based on this, the ages of stratum hiatus of the three unconformities U_2, U_3 and U_5 are about 0.93—0.84 Ma, 1.8—1.2 Ma and 5—3.66 Ma, respectively. Ages of U_1 and U_4 were estimated at ~ 0.14 Ma by sedimentation rates (Figs. 5 and 6).

Some fossil animals were found in the section or equivalent stratigraphy in other localities of the basin. Fossil stoneworts *Tectochaea*, *Kosmogyra ovalis* and *Charites huangi* sp. and fossil Ostracoda-gasteropod *Metacypris* sp., *Ostrea* sp., *Nyocypris* sp., *Chara* sp., *Plannorbis* sp., *Hydrobia* sp. and *Ancykes* sp. were found in the Shulehe Fm., mostly in the Gongxingshan and Getanggou Members of the studied section, and their ages are estimated as Miocene[1)][28]. Many fossil mammals were found in the Baiyanghe Fm. below the

1) Exploration and Exploitation Department of the Yumen Oil Field, The Tertiary in the Jiuquan Basin, 1990, unpublished report.

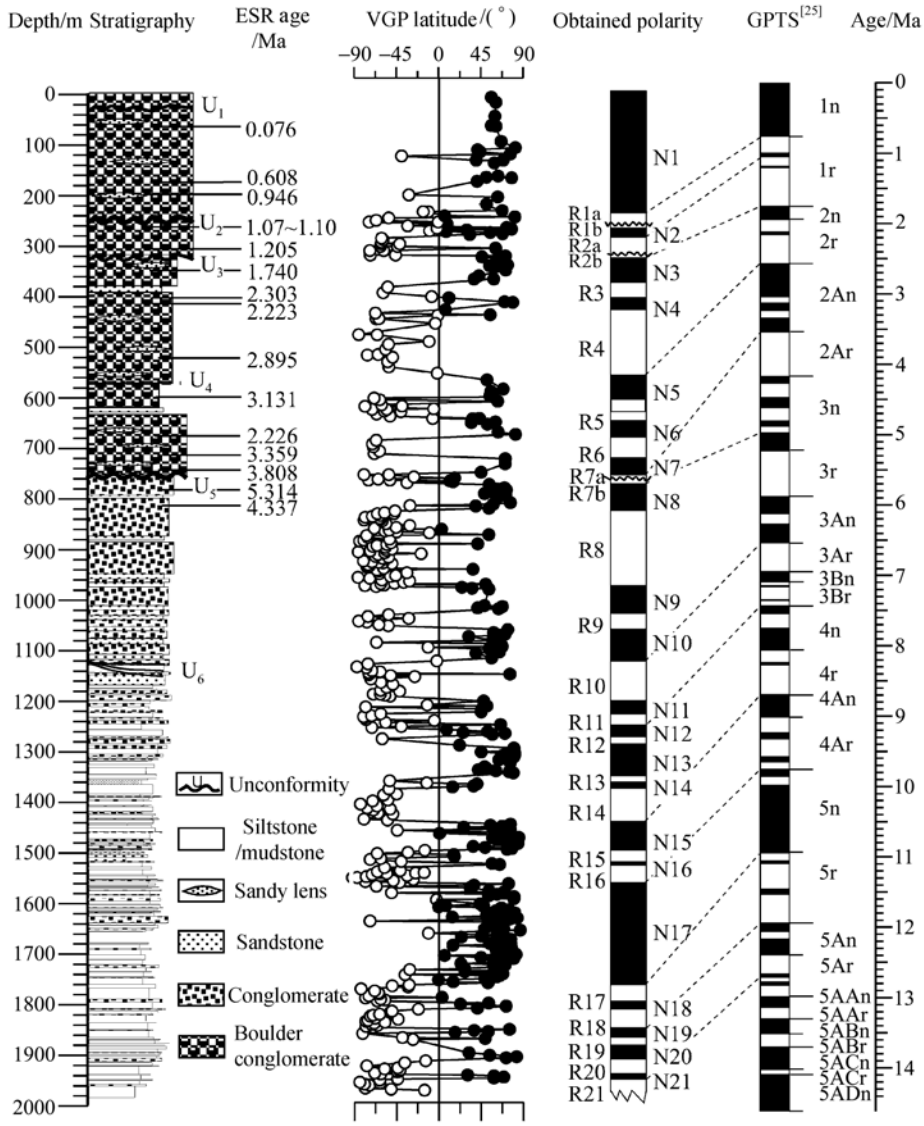

Fig. 5. Depth function of the paleomagnetic directions in the Laojunmiao section and correlation of the observed magnetic polarity zones with the geomagnetic polarity timescale[25]. ESR ages are from ref. [26].

Shulehe Fm. The recognized taxa include: *Tataromys grangeri*, *T. Sigmoden*, *Leptotataromys minor*, Parasminthus cf. *Asiae-centralis*, *P. tangingili*, *P. parvulus*, *Eucricetodon asiaticus*, *Desmatolagus* sp., *Sinolagomys* ? sp. and *Amphechinus* sp. Many of these are important members of the nearby famous Taben-buluk Fauna of the late Oligocene. Thus, the mammal association suggests the age of the stratigraphy is confined in the middle to late Oligocene[1)]. This mammal-suggested age is in good agreement with that determined by the paleomagnetism.

Three ESR ages at depths of 260, 257 and 255 m below U_4 indicate this part of the stratigraphy is at ~1.1 Ma, and this at depth 300 m is at 1.21 Ma[26], supporting the correlation of normal zone N2 with chron 1r.1n of the GPTS, i.e., the Jaramillo event at 0.99—1.07 Ma[25] (Fig. 5). Eight ESR ages from the

1) See footnote 1) on page 1047.

stratigraphy between unconformities U_3 and U_5 range from about 1.7 to 3.8 Ma, consistent with ages determined by paleomagnetism (Fig. 5). Furthermore, two ESR ages immediately below the unconformity U_5 also accord with those given by the interpreted normal zone N8, both at about 5 Ma (Fig. 5). Although present ESR dating still has relatively large errors, it appears to work successfully for the LJM section. This is also supported by the linear presentation of paired ESR ages and depths[26]. This means that the ages from ESR dating and interpreted magnetic polarities support each other.

Based on the paleomagnetism above, the ages of the main stratigraphic boundaries, the Getanggou and Niugetao Members, Yumen Conglomerate, Jiuquan Gravel Bed, and Gobi Gravel Bed, are >13−8.3, 8.3−< 4.9, 3.66−0.9, 0.8−0.14, and 0.14−0 Ma, respectively.

Figure 6 shows the age-depth relationship of all interpreted observed magnetic polarity zones and calculated main stratigraphic boundaries. A good linear pattern is established, except for the intervals at the place where unconformities occur. This indicates a reliable interpretation of the observed magnetic zones.

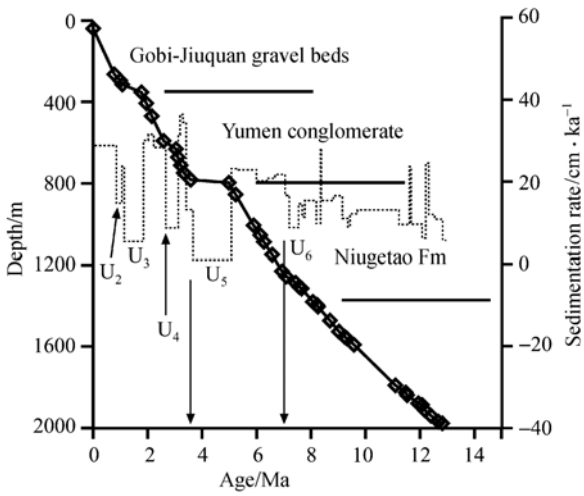

Fig. 6. Age-depth relationship for the interpreted magnetic polarity zones and calculated stratigraphic boundaries in the Laojunmiao section. Sedimentation rates are calculated and plotted against each two observed zones.

5 Stratigraphic evolution, main tectonic events and uplift of the northern Tibetan Plateau

The occurrences of the five unconformities at about 7−6.6 Ma, <4.9−3.66 Ma, <2.94−2.58 Ma, <1.8−1.23 Ma and 0.93−0.84 Ma are interpreted to five significant tectonic and plateau uplift events, as well as the impact of that tectonism on the sedimentary environment. According to sedimentary facies, the sedimentary evolution of the LJM section can be divided into five stages: >13−11 Ma as hemi-deep lake, 11.1−8.3 Ma as shallow lake, 8.3−6.6 Ma as combination of shallow lake and fan delta under dry climate, and 6.6−0 Ma as several cycles of alluvial fans[20]. Therefore, the combination of the sedimentary evolution and the occurrences of the unconformities implies that the northern Qilian Mountains began gradual slow uplift at about 8 Ma (with some accelerating since 6.6 Ma), causing a gradual turn of domination of lacustrine environment to subaerial alluvial fan environment via shallow lake-fan delta transitional environment, and forming the progressive unconformity U_6 and the initial LJM anticline. At least at about 3.66 Ma ago, the Plateau began rapid uplift. The accompanied strong compression led to a fast upheaval of the LJM anticline, deforming and denuding the stratigraphy and forming the angular unconformity U_5. Subsequent episodic compressions occurred at about <2.94−2.58 Ma, <1.8−1.23 Ma, 0.93−0.84 Ma and 0.14 Ma, and led to further intermittent uplift of the Plateau and folding of the LJM anticline, forming the unconformities U_4−U_1. Tectonism forming U_4 and U_2 also caused a big shift of paleo-river direction, i.e., firstly from previous northwesterly to dispersed or weak northeasterly directions at U_4, and then completely to northeasterly at U_2[20]. The Jiuquan Gravel Bed was ended at about 0.14 Ma with local deformation and denudation and strong river dissection of the stratigraphy, forming a partial unconformity near the anticline and several river terraces, reflecting a latest intermittent rapid uplift of the Qilian Mountains. A similar uplift process of the northern Qilian Mountains is clearly recorded as well by the change of sedimentation rate (Fig. 6). The sedimentation rate increases obviously since about 8−7 Ma from previous mean of

13.6 cm/ka to later mean of 27 cm/ka, and rapidly (~35－60 cm/ka) at about 3.66 Ma, but drops abruptly to near zero at the unconformities (Fig. 6).

The fission track thermo-history of apatite from foreland basins of the Qilian Mountains revealed that the Qilian Mountains began to uplift at Miocene time[29,30]. The study of river terraces since Pleistocene in the east Qilian Mountains showed that the Qilian Mountains was strongly uplifted and deformed at ~1.2 Ma, 0.8 Ma and 0.14 Ma, causing strong incision and forming various terraces[9,10,31]. Episodic uplift and deformation of the Guide, Xunhua and Linxia Basins in the northeast Tibetan Plateau were paleomagnetically dated to at ~8 Ma, 3.6 Ma, 2.6 Ma, 1.8 Ma, 1.2 Ma, 0.8 Ma and 0.14 Ma[5－7,32], synchronous to the uplift and deformation of the Qilian Mountains. Compared with the northeastern Tibetan Plateau, the northern Tibetan Plateau appears more sensitive to the tectonic compression exerted by the Indian plate and experienced stronger tectonism. But there is no sedimentary evidence to indicate a maximum elevation for the entire Plateau attained at ~ 8 Ma followed with a collapse of the Plateau[33]. Our evidence shows that a real large scale surface uplift began ~ 8 Ma, rapidly since ~ 3.6 Ma (manifested as several intermittent rapid uplifts), which led the Plateau rise up to its present height. In addition, our results also do not support the view of northeastward accretion of the NE Tibetan Plateau from which the northern Qilian Mountains was regarded to be formed latterly (~5 Ma)[11,12].

6 Conclusion

(1) The measured LJM section is paleomagnetically dated between 13 and 0 Ma, in which the Getanggou Member, Niugetao Members, Yumen Conglomerate, Jiuquan Gravel Bed, and Gobi Gravel Bed are dated in >13－8.3 Ma, 8.3－<4.9 Ma, 3.66－0.93 Ma, 0.84－0.14 Ma and 0.14－0 Ma, respectively.

(2) The uplift of the northern part of the Tibetan Plateau was nearly synchronous with that of its northeastern part; it began to gradually uplift at ~8.3－6.6 Ma from a lowland and rapidly uplift since ~3.66 Ma manifested as episodes of intermittent rapid intense uplifts at ~3.66 Ma, <2.94－2.58 Ma, <1.8－1.23 Ma, 0.93－0.84 Ma and 0.14 Ma. This late Miocene-Quaternary uplift has finally made the northern Tibetan Plateau attain its present height and the basin sediments changed gradually from fine lacustrine sandstone-mudstone to cyclic alluvial fanglomerates.

Acknowledgements We would like to thank Cao Jixiu, Ma Yuzhen, Chen Shiyue, Wu Guangjian, Chen Jianhua, Yang Shengli, Song Yougui, and Fu Kaidao for their field-work assistances. Many thanks should be also given to Prof. Zhu Rixiang at the Institute of Geology and Geophysics of CAS and Prof. Rob Van der Voo in the University of Michigan for their help in laboratory. Valuable comments are thankful from Drs. Karl-Heinz Wyrwoll and Bryan Krapez and Prof. Huang Baochun and an anonymity. This study was supported jointly by the NSFC (Grant No. 40334038, 40121303), the National Key Project for Basic Research on the Tibetan Plateau (Grant No. G1998040809) and CAS "Hundred Talents Project" (Grant No. Ren-Jiao-Zi[2000] 0282).

References

1. Johnson, N. M., Stix, J., Tauxe, L. et al., Paleomagnetic chronology, fluvial processes, and tectonic implications of the Siwalik deposits near Chinji village, Pakistan, Journal of Geology, 1985, 93: 27－40.
2. Burbank, D. W., Reynold,s G. H., Sequential late Cenozoic structural disruption of the northern Himalayan foredeep, Nature, 1984, 311: 114－118.[DOI]
3. Li, J. J., Fang, X. M., Uplift of Qinghai-Tibetan Plateau and environmental change, Chinese Science Bulletin, 1998, 44(23): 2217－2224.
4. An, Z. S., Wang, S. M., Wu, X. H. et al., Eolian evidence from the Chinese Loess Plateau: the onset of great late Cenozoic glaciation in the Northern Hemisphere and Qinghai-Xizang Plateau uplift forcing, Science in China, Ser. D, 1999, 42(3): 258－271.
5. L,i J. J., Fang, X. M., Ma, H. Z. et al., Geomorphologeical and environmental evolution in the upper reaches of Huang He during the Late Cenozoic, Science in China, Ser. D, 1996, 39(4): 380－390.
6. Fang, X. M., Li, J. J., Zhu, J. J. et al., Absolute age determination and division of the Cenozoic stratigraphy in the Linxia Basin, Gansu Province, China, Chinese Science Bulletin (in Chinese), 1997, 42(14): 1457－1471.
7. Li, J. J., Fang, X. M., Van der Voo, R. et al., Reconnaissance Late Cenozoic magnetostratigraphy (11－0 Ma) of the Wangjiashan section in the Longzhong Basin, western China: evidence for rapid mid-Pliocene uplift of the Tibetan Plateau, Geologie & Mijnbouw, 1997, 76: 121－134.
8. Zheng, H. B., Powell, C. M., An, Z. S. et al., Pliocene uplift of the northern Tibetan Plateau, Geology, 2000, 28(8): 715－718.[DOI]

9. Yang, J. C., Tan, L. H., Li, Y. L. et al., River terraces and neotectonic evolution at north margin of the Qilian Mountains, Quaternary Sciences (in Chinese), 1998, (3): 229－237.
10. Li, Y. L., Yang, J. C., Tan, L. H. et al., Impact of tectonics on alluvial landforms in the Hexi Corridor, Northwest China, Geomorphology, 1999, 28: 299－308.[DOI]
11. Meyer, B., Tapponnier, P., Bourjot, L. et al., Crustal thickening in Gansu-Qinghai, lithospheric mantle subduction, and oblique, strike-slip controlled growth of the Tibet Plateau, Geophysics Journal International, 1998, 135: 1－47.[DOI]
12. Tapponnier, P., Molnar, P., Active faulting and tectonics in China, Journal of Geophysical Research, 1977, 82: 2905－2930.
13. Li, Y. T., The Tertiary of China (in Chinese), Beijing: Geological Publishing House, 1984, 47.
14. Sun Jianchu, Synopsis for geology of the Qilianshan region, Geological Review (in Chinese), 1942, 7(1-3): 17－25.
15. Yu Boliang, Characteristic and significance of neotectonism in the Gansu Corridor, The Records of the First Symposium on Neotectonic Movements of the Chinese Academy of Sciences (in Chinese), Beijing: Science Press, 1957, 119－126.
16. Song Zhichen, Spore assemblage in the Tertiary redbed at Jiuquan, Gansu and its significance in geology and botany, Acta Palaeontologica Sinica (in Chinese), 1958, 6(2): 159－166.
17. Huang, H. F., Peng, Z. L., Lu, W. et al., Paleomagnetic division and comparison of the Tertiary system in Jiuxi and Jiudong Basins, Acta Geologica Gansu (in Chinese), 1993, 2(1): 6－16.
18. Tan, L. H., Yang, J. C., Duan, F. J., Stages of Cenozoic Tectonic Movement in Hexi Corridor, Gansu Province, Acta Scientiarum Naturalium, Universitatis Pekinensis (in Chinese), 1998, 34(4): 523－532.
19. Chen J., Lu Y. C., Ding G. Y., Stages of Quaternary tectonic movement in west Qilianshan Mountain and Jiuxi Basin, Quaternary Sciences (in Chinese), 1996, 16(3): 263－271.
20. Song Chunhui, Fang Xiaomin, Li Jijun et al., Tectonic uplift and sedimentary evolution of the Jiuxi Basin in the northern margin of the Tibetan Plateau since 13 Ma BP, Science in China, Ser. D, 2001, 44 (Supplement): 192－202.[Abstract][PDF]
21. Riba, O., Systectonic unconformities of the Alto Cardener, Spanish Pyrenees: a genetic interpretation, Sedimentary Geology, 1976, 15: 213－233.
22. McElhinny, M. W., Statistical significance of the fold test in paleomagnetism, Geophys. J. Roy. Astron. Soc., 1964, 8: 338－340.
23. Tauxe, L., Paleomagnetic Principles and Practice, Dordrecht: Kluwer Academic Publishers, 1998, 299.
24. Tauxe, L., Gallet, Y., A jackknife for magnetostratigraphy, Geophysical Research Letters, 1991, 18(9): 1783－1786.
25. Cande, S. C., Kent, D. V., Revised calibration of the geomagnetic polarity timescale for the Late Cretaceous and Cenozoic, Journal of Geophysical Research, 1995, 100: 6093－6095.[DOI]
26. Shi, Z. T., Ye, Y. G., Zhao, Z. J. et al., ESR dating of the Late Cenozoic molassic deposits in the Jiuxi Basin, Science in China, Ser. D, 2001, 44(Supplement): 203－209. [Abstract][PDF]
27. Zhao, Z. J., Fang, X M, Li, J. J. et al., Paleomagnetic dating of the Jiuquan Gravel in the Hexi Corridor: Implication on the mid-Pleistocene uplift of the Qinghai-Tibetan Plateau, Chinese Science Bulletin, 2001, 46(14): 1208－1212.
28. Wang Shui, Cenozoic stoneworts in the Jiuquan Basin, Gansu, Acta Palaeontologica Sinica (in Chinese), 1965, 13(3): 463－509.
29. George, A. D., Marshallsea, S. J., Wyrwoll, K., et al., Miocene cooling in the northern Qilian Shan, northeastern margin of the Tibetan Plateau, revealed by apatite fission-track and vitrinite-reflectance analysis, Geology, 2001, 29(10): 939－942.[DOI]
30. Jolivet, M., Brunel, M., Seward, D. et al., Mesozoic and Cenozoic tectonics of the northern edge of the Tibetan Plateau: fission tract constraints, Tectonophysics, 2001, 343(1-2): 111－134.[DOI]
31. Pan, B. T., Wu, G. J., Wang, Y. X. et al., Age and genesis of the Shagou River terraces in eastern Qilian Mountains, Chinese Science Bulletin, 2001, 46 (6): 509－513.[Abstract][PDF]
32. Pan, B. T., Li, J. J., Cao, J. X. et al., The Geomorphology evolution of the Hulong Basin and the development of the Yellow River study, Mountain Research (in Chinese), 1996, 14 (3): 153－158.
33. Harrison, T. M., Copeland, P., Kidd, W. S. F. et al., Raising Tibet, Science, 1992, 255: 1663－1670.